Journal of Catalysis 295 (2012) 133–145

Contents lists available at SciVerse ScienceDirect

Journal of Catalysis

journal homepage: www.elsevier.com/locate/jcat

Active sites and reactive intermediates in the hydrogenolytic cleavage of C–C bonds in cyclohexane over supported iridium

Hui Shi, Xuebing Li, Gary L. Haller, Oliver Y. Gutiérrez, Johannes A. Lercher *

Department of Chemistry and Catalysis Research Center, Technische Universität München, Lichtenbergstrasse 4, D-85747 Garching, Germany

ARTICLE INFO

Article history:
Received 8 June 2012
Revised 14 July 2012
Accepted 6 August 2012
Available online 23 September 2012

Keywords:
Iridium
Cyclohexane
Ring opening
Hydrogenolysis
Structure sensitivity

ABSTRACT

Hydrogenolysis of cyclohexane has been explored over supported Ir catalysts. The kinetic data are combined with modeling results to assess the structural requirements and the nature of catalytically relevant surface intermediates for endocyclic C–C bond cleavage. The turnover frequency (TOF) for cyclohexane hydrogenolysis showed complex dependence on Ir particle size, while the selectivity to the primary ring opening product, *n*-hexane, decreased monotonically with decreasing Ir dispersion. The decreasing TOF as the Ir dispersion decreased from 65% to 52% originates principally from the diminishing abundance of low-coordination Ir atoms at particle surfaces. The increase of the TOF with further Ir particle growth is attributed to an increased fraction of terrace planes, or step sites, and a less unsaturated nature of the most abundant reactive intermediate. Selectivities for multiple C–C bond cleavage, yielding $C_{<6}$ alkanes, varies with the relative abundance of coordinatively unsaturated Ir atoms and terrace planes. The multiple hydrogenolysis depends additionally upon H_2 pressure, because single and multiple C–C bond scissions are mediated by surface intermediates with different H-deficiencies.

1. Introduction

The hydrogenolysis of cycloalkanes holds immense practical and fundamental relevance. Selective ring opening is an important process following deep hydrogenation of aromatics during the upgrading of light cycle oil (LCO) for blending in the diesel pool [1–3]. From a fundamental standpoint, the active site requirements and the elementary steps involved in the hydrogenolysis of paraffinic C–C bonds remain partly unresolved for acyclic alkanes even after decades of studies [4], not to mention the much less explored cycloalkanes in this respect.

The structure sensitivity of hydrogenolysis of C–C bonds in alkanes was first demonstrated by Sinfelt et al. for ethane hydrogenolysis over Ni–Cu alloys [5]. Since then, alkane hydrogenolysis is usually assumed to require a large ensemble, though the evidence arising from particle size effects is actually sparse and contradictory [6–18]. Although iridium is known to possess high hydrogenolysis activity, the structure sensitivity for C–C (σ-) bond hydrogenolysis over Ir catalysts is less explored and far from established. Foger and Anderson reported ranges of less than three times in specific activities for ethane hydrogenolysis on Al_2O_3- and SiO_2-supported Ir catalysts with average particle sizes of 1.5–7.0 nm [11]. Across a much wider variety of reaction conditions, Engstrom et al. found structure sensitivity for hydrogenolysis of ethane or butanes over Ir(1 1 1) and Ir(1 1 0)-(1 × 2) surfaces [12–14]. In contrast, little change in the TOF was observed for *n*-butane hydrogenolysis on Ir/SiO_2 [11], as also for cyclopentane ring opening on Ir/Al_2O_3 [15].

Compared to the extensively studied ring opening reaction of methylcyclopentane (MCP) [19–26], far less fundamental knowledge is available for the direct endocyclic C–C bond cleavage of the more stable C_6-naphthenic structures, which are more abundant in LCO feeds. Due to the low reactivity of the cyclohexyl ring, bifunctional catalysts, which supply an acid-catalyzed ring contraction step to more reactive cyclopentyl backbones, are more often employed [1,27–32]. Catalyst optimization in such a "bifunctional" scenario requires both a delicate metal–acid balance [29,32] and tuning of metal particle size. This complexity hampers attempts to establish an unequivocal structure–performance relationship with respect to the metal component.

Pt is effective for ring opening in combination with acidic zeolites [27], but, in the absence of appropriate Brønsted acidity, catalyzes predominantly dehydrogenation and isomerization reactions of six-membered rings [4]. Monometallic Ru- and Pd-based catalysts exhibit too high and too low ability, respectively, to cleave C–C bonds. Non-acidic Ir-based catalysts hold promise among the monofunctional metal catalysts for achieving selective ring opening of six-membered naphthenes in a single, direct scission [1], as long as C–C bond ruptures at unwanted positions and for multiple times are minimized. In a recent study, Resasco and coworkers found intriguing trends concerning different endocyclic

* Corresponding author. Fax: +49 89 28913544.
E-mail address: johannes.lercher@ch.tum.de (J.A. Lercher).

0021-9517/$ - see front matter © 2012 Published by Elsevier Inc.
http://dx.doi.org/10.1016/j.jcat.2012.08.005

C–C bond cleavage modes of di-substituted cyclohexanes over a series of monofunctional Ir catalysts on non-acidic or weakly acidic supports [33]. This study pointed to the possibility of maximizing C–C bond ruptures at hindered positions, thus raising cetane number, by tailoring Ir dispersion and support characteristics. Nevertheless, the kinetic features of such systems, especially those associated with changes in H_2 pressure, remain unexplored.

A detailed kinetics study on the hydrogenolysis of cyclohexane, a model six-membered naphthenic molecule, has been undertaken, therefore, using Ir particles of different sizes supported on non-acidic carriers and a wide range of reaction conditions. The catalytic consequences of Ir dispersion and H_2 pressure have been addressed in regard to turnover rates and selectivities to ring opening, and internal and terminal modes of multiple hydrogenolysis. Mechanistic and structural origins for cyclohexane hydrogenolysis on Ir particle surfaces are discussed. To augment previous knowledge accumulated on bifunctional Ir catalysts, where a delicate acid-metal balance is more important than metal characteristics [29,32,34], the present study explicitly addresses the catalytic role of metallic Ir in the hydrogenolysis of endocyclic C–C bonds.

2. Experimental section

2.1. Catalyst preparation

2.1.1. Ir/Al_2O_3 catalysts from Cl-free precursor

A Cl-free precursor, iridium(III) acetylacetonate ($Ir(acac)_3$, Aldrich, 97%), was dissolved in toluene [35]. Fumed γ-alumina (Alu C, Evonik Degussa) was the support. In a typical procedure of incipient wetness impregnation, aliquots of the solution were added dropwise to γ-Al_2O_3 while stirring with a quartz rod. The as-prepared sample was dried in synthetic air (Westfalen, 20.5 vol.% O_2 in N_2) at 393 K overnight and then treated in H_2 (Westfalen, 99.999%) at 723 K for 5 h. The reduced material was divided into six portions treated at varying temperatures (473–873 K) for 5 h in dry synthetic air flow and then again in H_2 at 723 K for 4 h. A temperature increment of 1 K min^{-1} was applied for all thermal treatments, whereas flow rates of 100 cm^3 (STP) min^{-1} (g-sample)$^{-1}$ were applied for all gases. Catalyst samples are denoted as *m*%Ir(*D*)–1/Al_2O_3, where *m*%, *D* and 1 are the actual Ir loading by wt.% determined by ICP-OES, the fractional Ir dispersion measured by H_2 chemisorption and a designation of the Cl-free precursor, respectively.

2.1.2. Ir/Al_2O_3 catalysts from Cl-containing precursor

Ammonium hexachloroiridate ($(NH_4)_2IrCl_6$, Aldrich, 99.99%) was used as another Ir source to examine the potential effect of precursor on the catalytic performance. The procedure for incipient wetness impregnation was the same as for Series-1 catalysts except that the precursor was dissolved in doubly-distilled deionized water. After impregnation, the samples were Parafilm covered at ambient conditions overnight, and then dried in synthetic air at 393 K overnight and reduced in H_2 at 723 K for 5 h. This batch was then divided into four aliquots, which were treated at different temperatures (673–823 K) for 5 h in dry synthetic air flow and reduced at 723 K for 4 h in pure H_2 flow. A high-Ir-loading sample was prepared by wetness impregnation using the same $(NH_4)_2IrCl_6$ solution at a fivefold excess volume relative to that in incipient wetness impregnation. After evaporating the solution in a rotavap and drying at 393 K for 12 h, the high-loading sample was reduced at 723 K for 4 h in pure H_2 flow without air-calcination. A temperature increment of 1 K min^{-1} was applied for all thermal treatments, whereas flow rates of 100 cm^3 (STP) min^{-1} (g-sample)$^{-1}$ were applied for all gases. Samples thus obtained are denoted as *m*%Ir(*D*)–2/Al_2O_3, *m*%, *D* and 2 are the actual Ir loading by wt.% determined by ICP-OES, the fractional Ir dispersion obtained from H_2 chemisorption measurements, and a designation of the Cl-containing precursor, respectively. In addition, a sample was prepared on SiO_2 support (Aerosil 200, Evonik Degussa) using $(NH_4)_2IrCl_6$ and incipient wetness impregnation.

2.2. Catalyst characterizations

2.2.1. H_2 chemisorption and N_2 physisorption

Weakly and strongly adsorbed fractions of H_2 uptakes were determined volumetrically by a Sorptomatic 1990 instrument. Catalyst samples were pretreated in 100 kPa of static H_2 at 723 K for 2–3 h and then evacuated at the same temperature for 0.5 h before measurements. H_2 adsorption was conducted at 307 K in a pressure range of 0.5–13.2 kPa with an equilibrating time of 2–5 min for each pressure increase step. After completing the first isotherm, the sample was evacuated to 10^{-4} kPa for 1 h and a second isotherm measured physisorption. The second isotherm was subtracted from the first one. The amount of chemisorbed hydrogen was determined by extrapolating the linear part of the difference isotherm ($P > 6.5$ kPa) to zero pressure. Dispersions (*D*), defined as the fraction of Ir atoms exposed at surfaces, were calculated by assuming $H_{strong}/Ir = 2$ [36–38]. This ratio was rationalized by multiple hydrogen adsorption on coordinatively unsaturated surface Ir atoms [38]. The strong H_2 adsorption on bare γ-Al_2O_3, pretreated in the same way as the catalysts, was negligible.

The porosity of the catalyst samples was measured by N_2 physisorption at 77 K on the Sorptomatic 1990 instrument. Prior to the measurements, samples were outgassed at 523 K for 2 h. The specific surface area was calculated by applying BET theory [39] to the adsorption isotherms over a relative pressure range (p/p^0) between 0.03 and 0.10, assuming a cross-sectional area of 0.162 nm^2 for a N_2 molecule.

2.2.2. Transmission electron microscopy

Transmission electron microscope (TEM) images of the materials were recorded with a JEM-2010 JEOL transmission electron microscope operating at 120 kV. Before being transferred to the vacuum system, the samples were ground, suspended in ethanol and ultrasonically dispersed for 2 min. Drops of the dispersions were applied on a copper grid-supported carbon film.

2.2.3. ICP-OES

The Ir contents of the samples were determined by inductively-coupled plasma optical emission spectroscopy (ICP-OES). Before measurement, 60–100 mg of the solid sample was mixed with hydrofluoric acid (2.0 cm^3, 10 wt.%), hydrochloric acid (0.3 cm^3, 38 wt.%) and nitric acid (0.1 cm^3, 69 wt.%), and boiled until the solution was clear. The Ir concentration of the solution was measured on a Spectroflame FTMOA81A ICP-OES spectrometer (Spectro Analytic Instruments). Standard solutions containing 0, 50, 100, and 200 ppm Ir in diluted nitric acid (25 cm^3, 6.5 wt.%) were used for calibration.

2.2.4. XRD

The XRD diffractograms of selected catalysts were recorded with a Philips X'Pert Pro System (Cu Kα1-radiation, 0.154056 nm) operating at 45 kV and 40 mA. Measurements were carried out using a step size of 0.017° (2θ) and 1400 s as count time per step.

2.3. Steady-state kinetic measurements

The hydrogenolysis of cyclohexane (CH) was studied in a stainless steel packed-bed tubular reactor. Compacted and crushed catalyst powders sieved to 180–280 μm were diluted with appropriate amounts of acid-washed quartz sand of identical sieve

fractions to ensure sufficient bed lengths for plug-flow hydrodynamics. A K-type thermocouple was attached to the external surface of the reactor within the isothermal region to measure and control reaction temperatures. Less than 1 K difference was found between temperatures measured on the surface of the reactor or within the catalyst bed. Preliminary tests had confirmed the absence of transport artifacts (Fig. S1). Prior to reactions, catalysts were pretreated in a pure H_2 flow of 20 cm^3 (STP) min^{-1} (from room temperature to 623 K, 10 K min^{-1} ramp and holding for 2 h) and then cooled to the reaction temperature (503–563 K). CH was introduced using a flow of He (Westfalen, 99.996%) passing through a series of bubblers (in a thermostatted water bath) which contained liquid CH (Aldrich, ⩾99%). The He flow carrying CH vapor saturated at the bath temperature mixed with a flow of H_2 (Westfalen, 99.999%) in a co-current mode and contacted the catalyst bed to initiate the reaction. Flow rates of gases and total pressures of the reactor system were modulated by electronic mass flow controllers (Bronkhorst) and back pressure regulators (Bronkhorst). The kinetic measurements were conducted under total pressures of 0.1–2.0 MPa with the H_2/CH ratio varying from 20 to 350. The products were analyzed online by a Hewlett–Packard 6890 Plus GC equipped with a DB Petro column (320 μm × 100 m) connected to a flame ionization detector. All lines downstream from the saturator to the GC were heated to 393 K to ensure no condensation of either the reactant or the products. Initial rates and selectivities were reported as values derived by extrapolation of measured rates and selectivities to zero contact time. There was no detectable reaction on bare supports or in the absence of the catalyst. During high pressure experiments, deactivation of low-dispersion catalysts, to the maximum extent of 15%, was observed after 5 days below 543 K. In the majority of cases, the deactivation was kept below 10% during the whole run lasting more than 10 h.

3. Results

3.1. Catalyst characterizations

The effect of calcination temperature on Ir dispersion is shown in Fig. 1. Increasing the calcination temperature from 393 to 873 K decreased the Ir dispersion from ca. 60% to lower than 20% for the low-loading (0.50–0.54 wt.% Ir) samples. The Ir/Al_2O_3 samples prepared from Cl-free precursor featured a sharp loss of Ir dispersion from 52% to 24% between 623 and 673 K, possibly because of enhanced mobility of surface iridium oxide close to the Tammann temperature of IrO_2, 686 K. By contrast, the Ir dispersion of those prepared from Cl-containing precursor showed a relatively gradual decrease and began to approach that of the Cl-free counterpart at high calcination temperatures (>800 K). The presence of chlorine is responsible for re-dispersion of Ir and Pt in O_2-containing atmosphere [40,41].

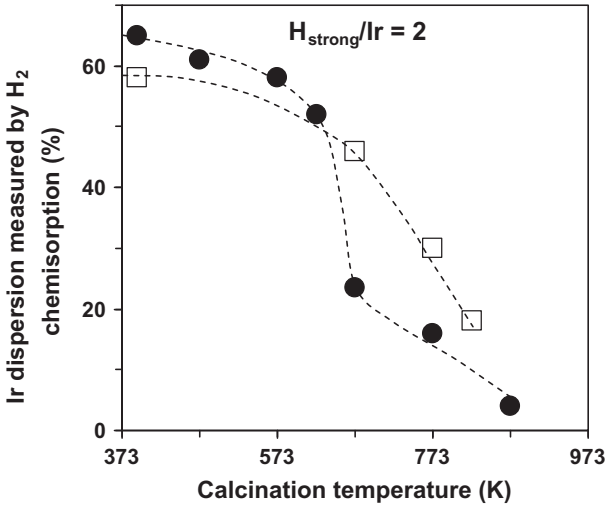

Fig. 1. Ir dispersion as a function of calcination temperature in synthetic air. Filled circles represent the dispersions of low-loading Ir/Al_2O_3 catalysts prepared from Cl-free precursor and empty squares correspond to those prepared from a Cl-containing precursor.

BET surface areas and Ir dispersions for all catalysts used in the kinetic studies are listed in Table S1 (Supporting information). Up to an Ir loading of ca. 2 wt.%, the surface areas of the catalysts were lower by at most 10% relative to bare Al_2O_3 support (104 m^2 g^{-1}). Neither air-calcination at 393–873 K nor H_2-reduction at 723 K altered to a remarkable extent the BET surface areas of the Ir/Al_2O_3 samples.

Representative TEM micrographs are presented in Fig. S2. Small (1–2 nm) Ir particles seemed to be prevalent on high-dispersion catalysts (Fig. S2a and b). For 1.92%Ir(0.11)/Al_2O_3 (Fig. S2f), a surface-weighted mean particle size was 11.7 ± 6.9 nm by sampling 210 Ir particles counted from 24 different areas. This value corresponds to $D = 0.09$ ($D = 0.99/d$ for spherical Ir particles [42]). For low-loading (0.50–0.54 wt.% Ir) samples, however, a sufficient number of visible particles were not available for analysis of particle size distribution. The XRD patterns of selected catalysts ($D = 0.235$, 0.11, 0.035) are shown in the Supporting information (Fig. S3). The average crystallite sizes calculated according to the Debye–Scherrer equation were in good agreement with the average particle sizes estimated from TEM and H_2 chemisorption measurements. A detailed discussion on the consequence of assumed H/Ir_s stoichiometry to the results reported in this study has been placed in the Supporting information.

The slow deactivation (ca. 10% after >10 h, see Section 2) suggests that the particle growth must have been not remarkable during the reaction. TEM photos were taken for catalysts after reactions; the result of one spent sample (Fig. S2c, Supporting information) hardly showed any difference in the particle size compared to that before reaction. Two spent catalysts ($D = 0.16$ and 0.52) were collected after several catalytic runs in order to have a sufficient amount for H_2 chemisorption. The results revealed <10% decrease in dispersion for both samples. Therefore, the Ir/Al_2O_3 catalysts were stable under elevated H_2 pressures, moderate temperatures, and high H_2/HC ratios.

3.2. An overview of reaction channels in cyclohexane conversion

Methylcyclopentane (MCP), a potential product from ring contraction (RC) of cyclohexane (CH), was observed only in traces (<0.3% within converted fractions) over all Ir catalysts studied (including Ir black). This is indicative of a negligible contribution of indirect ring opening (RO) following RC catalyzed by acid functions. Do et al. also concluded that indirect RO makes little contribution to the overall conversion of dimethylcyclohexane on Al_2O_3-, SiO_2-, and TiO_2-supported Ir catalysts [33]. If MCP were formed and rapidly ring-opened, methylpentanes would have been found in much larger quantities compared to *n*-hexane, due to the well-known preference of Ir to cleave unsubstituted C–C bonds [19]. Here, *n*-hexane was >95% within ROPs. This was equally true over catalysts synthesized with or without Cl. Thus, residual chlorine in the catalyst, associated either with Al_2O_3 or with surface Ir atoms, did not introduce an additional acid-catalyzed pathway for CH conversion. The reactions detected were isomerization, dehydrogenation, and hydrogenolysis (Scheme 1). Their relative significance depended on the H_2 pressure and temperature, as well as the Ir dispersion. The basic thermodynamic and kinetic characteristics of

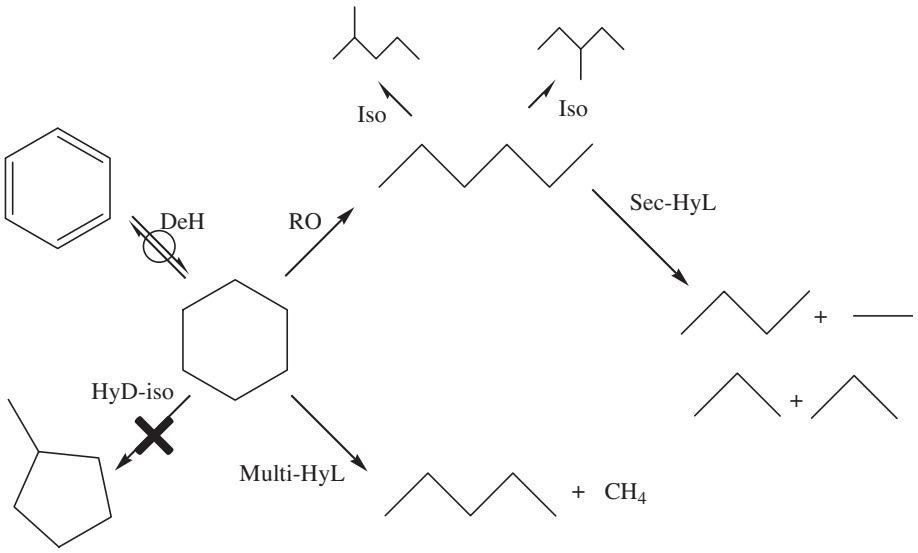

Scheme 1. Reaction network of CH conversion over Ir/Al_2O_3 catalysts in presence of high H_2 pressure. Minor modes of multiple-scissions in primary and secondary hydrogenolysis are not shown for brevity. DeH = dehydrogenation, RO = ring opening, Iso = isomerization (metal-catalyzed), HyD-iso: Hydroisomerization (acid-catalyzed), Multi-HyL: multiple hydrogenolysis, Sec-HyL: secondary hydrogenolysis.

the first two minor reaction channels are described in the Supporting information, while the hydrogenolytic scission of C–C bonds is the focus in the sections to follow.

3.3. Structure sensitivity of cyclohexane hydrogenolysis: rates and selectivities

Cyclohexane turnovers showed >95% selectivity to RO and fragmentation at H_2 pressures sufficiently high to suppress aromatization and isomerization (Section S2, Supporting information). The hydrogenolysis reactions possess high equilibrium constants (on the order of 10^2 for RO, and of 10^6–10^8 for fragmentation in the studied temperature range) and are, therefore, irreversible in light of their overall remoteness from equilibrium (approach-to-equilibrium index [43]: $\eta_{RO} < 10^{-3}$ and $\eta_{frag} < 10^{-9}$) at all conditions. *n*-Hexane was practically the exclusive ROP (>98% within C_6-isomers) from CH, whereas lighter *n*-alkanes, arising from multiple C–C bond cleavages of CH and secondary hydrogenolysis of re-adsorbed *n*-hexane, appeared in small quantities depending on the temperature, H_2 pressure, Ir dispersion, and contact time.

3.3.1. General trend of the activity-dispersion relation

Fig. 2 displays the mass-specific rates and turnover frequencies (TOFs) for hydrogenolysis of CH over Ir/Al_2O_3 catalysts as a function of Ir dispersion. Fig. S9 shows the CH turnover rates at 543 K over all studied Ir catalysts, including a purchased Ir black ($D = 0.01$) and $1.0\%Ir/SiO_2$ ($D = 0.20$). At both temperatures, the turnover rate first declined with decreasing Ir dispersion in a range corresponding to average particle sizes between 1 and 2 nm, then increased again when further decreasing Ir dispersion to lower than 30% (Fig. 2b and S9). Noting the higher mass-specific rate on $Ir(0.16)/Al_2O_3$ than on $Ir(0.24)/Al_2O_3$ (Fig. 2a), we exclude the reason for the variation of TOFs in the low-dispersion range to be related to an inaccurately determined number of surface Ir atoms. In marked contrast with the current monofunctional catalytic system, the TOFs for tetralin hydroconversion (RO plus RC) over bifunctional Ir/amorphous silica–alumina catalysts remained essentially constant in an Ir size range of 1.5–7.8 nm, suggesting that metal component in these catalysts was not involved in the rate-controlling step [32].

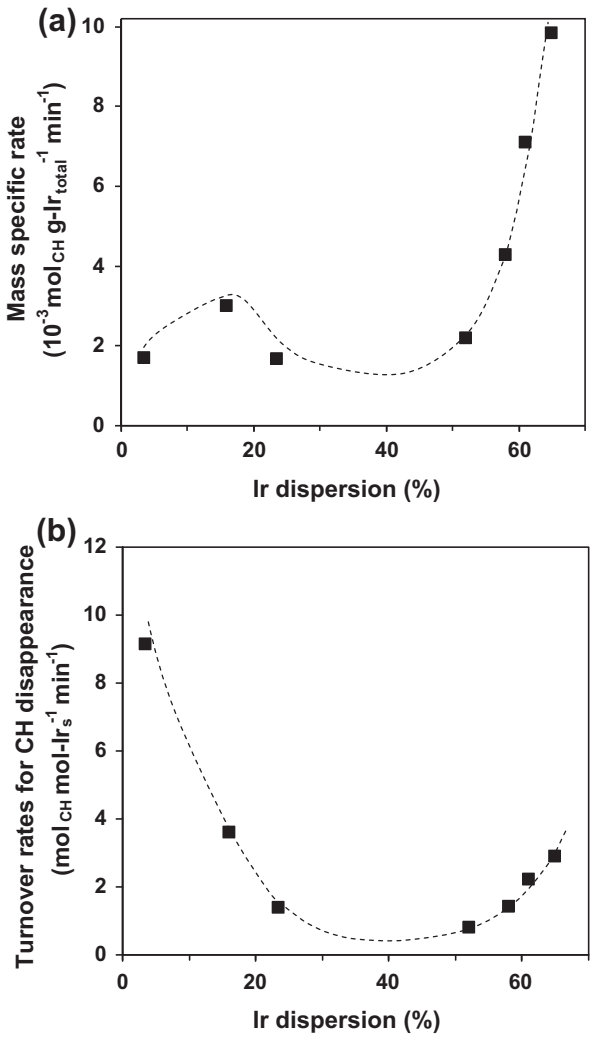

Fig. 2. Apparent dispersion sensitivities of (a) total-Ir-mass-based rates and (b) surface-exposed-Ir-based rates for cyclohexane (CH) hydrogenolysis at 523 K, 3.1 kPa CH and 0.56 MPa H_2 on $0.50\%Ir(D)$–$1/Al_2O_3$ catalysts.

3.3.2. Product selectivities: primary and secondary pathways

Space velocities were varied to probe the kinetic primary and secondary nature of different C–C bond cleavage products. The selectivities to *n*-hexane and *n*-pentane/methane extrapolated to zero conversion (Figs. 3 and S10) indicate that these are primary products, irrespective of the catalyst. In contrast, the selectivity trends for *n*-butane, propane, and ethane indicate that they are produced mainly via secondary reactions of re-adsorbed *n*-hexane. However, their formation via multiple hydrogenolysis of CH before desorbing the primary product *n*-hexane seems also plausible, in view of their non-zero selectivities at zero contact time. The selectivities to *n*-pentane and methane were insensitive to conversions over catalysts of low Ir dispersions. This suggests that secondary reactions of re-adsorbed *n*-hexane proceed mainly via internal C–C bond cleavages while largely bypassing terminal cleavage pathway.

Clearly, the catalysts that contain primarily small and large Ir particles substantially differ between each other in terms of the initial selectivities to *n*-pentane and methane, pointing to enhanced probability of terminal hydrogenolysis (of intermediately formed *n*-hexane before desorption) on larger Ir particles. The increased preference for successive terminal scission over lower-dispersion catalysts was manifested in the larger disparity of the initial pentane to methane ratio, for example, 0.6–0.8 (methane excess).

The initial selectivity to *n*-hexane increased with increasing Ir dispersion, as shown in Fig. 4a. The selectivity shown on an iridium

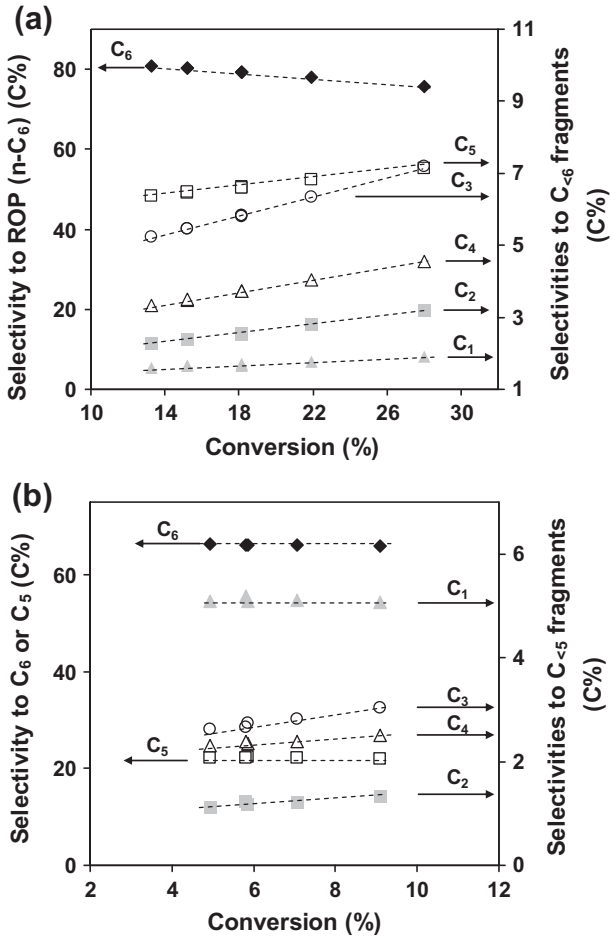

Fig. 3. Product selectivities as a function of conversion for the hydrogenolysis of cyclohexane (CH) over (a) 0.50%Ir(0.65)–1/Al_2O_3 and (b) 0.50%Ir(0.16)–1/Al_2O_3 at 523 K, 3.1 kPa CH and 0.56 MPa H_2. The contact time varied from 3.2 to 7.5 s (mol-Ir_s mol_{CH}^{-1}) in (a) and from 0.9 to 1.9 s (mol-Ir_s mol_{CH}^{-1}) in (b).

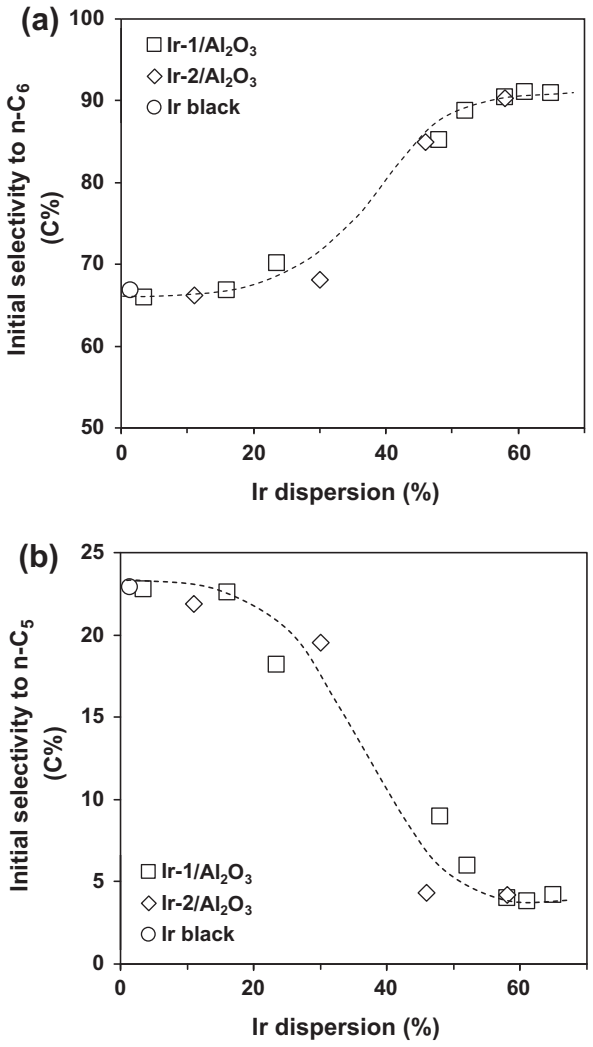

Fig. 4. Initial selectivities to (a) *n*-hexane and (b) *n*-pentane in hydrogenolysis of cyclohexane (CH) as a function of Ir dispersion at 523 K, 3.1 kPa CH and 0.56 MPa H_2 over Ir/Al_2O_3 catalysts prepared from Cl-free (□) and Cl-containing (◇) precursors and over commercial Ir black (○).

black (D = 0.01) was the same as that on supported Ir particles with the largest average size (D = 0.04). By contrast, the initial selectivity to *n*-pentane, which is formed via terminal hydrogenolysis of the ring-opened intermediates before desorption, decreased with increasing dispersion (Fig. 4b). For both *n*-hexane and *n*-pentane, plateaus were observed toward the low and high ends of the studied dispersion range. These plateaus suggest the selectivity limits at given reaction conditions over terrace planes and low-coordination atomic arrangement, which are the prevalent surface structures on large and small particles, respectively. Initial selectivities to ethane, propane, and *n*-butane that are formed via internal cleavages remained low (ca. 4–6%), and also decreased slightly with increasing dispersion.

3.4. H_2-pressure dependences of rates, reaction orders and selectivities over Ir particles of different sizes

Fig. 5 depicts the impact of Ir dispersion on the conversion rate as a function of H_2 pressure. The H_2 pressure, at which the maximal rates were observed, as well as the steepness of rate decline after the optimum pressure, differs significantly between smaller (D > 0.50) and larger particles (D < 0.25). The activity ratios among

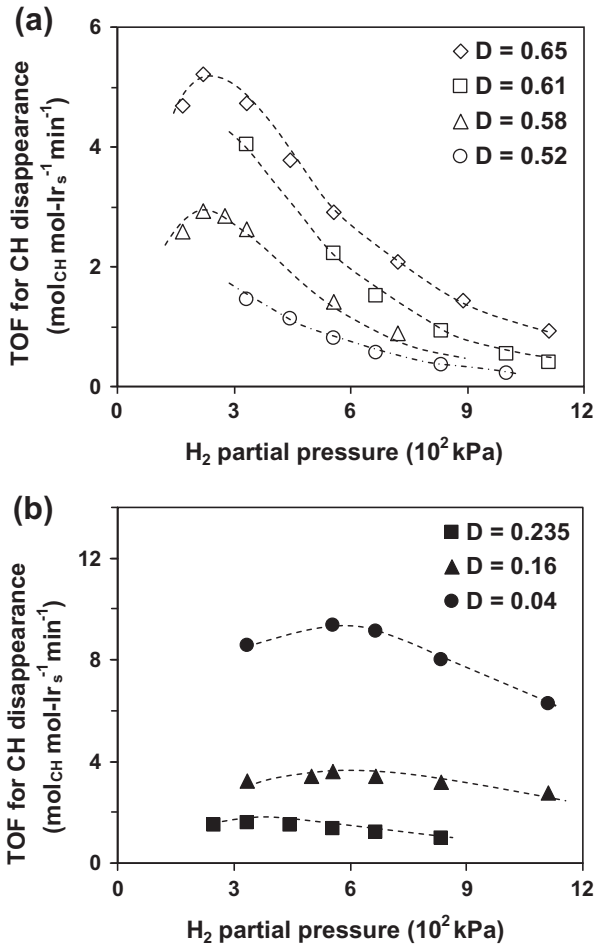

Fig. 5. Turnover rate dependences on H_2 pressure over 0.50%Ir(D)–1/Al_2O_3 catalysts with fractional dispersions of (a) 0.52–0.65 and (b) 0.035–0.235 at 523 K, 3.1 kPa cyclohexane (CH).

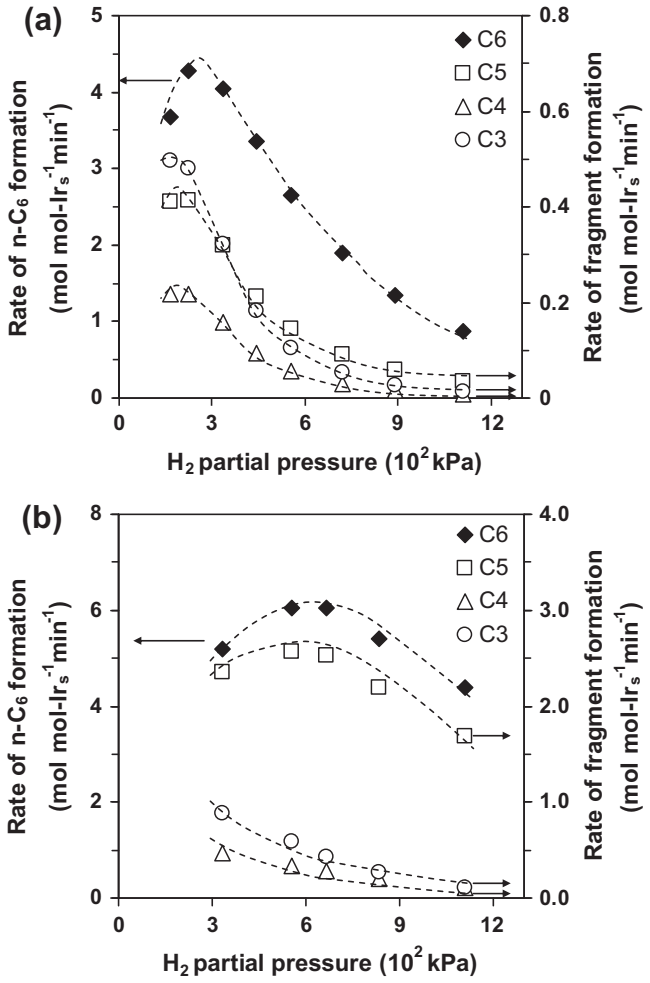

Fig. 6. Rate dependences on H_2 pressure of the ROPs, *n*-hexane (♦) and fragments, *n*-pentane (□), *n*-butane (△), and *n*-propane (○) over Ir-1/Al_2O_3 catalysts with Ir dispersion of (a) 0.65 and (b) 0.035, respectively. Reaction conditions were 523 K, 3.1 kPa CH. Rates were reported as values obtained after extrapolation to zero contact time. Formation rates of CH_4 and C_2H_6, revealing similar trends as their pairing products (C_5H_{12} and C_4H_{10}, respectively) with changes in H_2 pressure, are omitted for the sake of clarity.

different catalysts that contain small Ir particles were constant at any given H_2 pressure (Table S2, Supporting information), indicating the same H_2 pressure dependences of TOFs for all of these small particles. For large Ir particles (Fig. 5b), the H_2 pressure for maximum TOFs shifted higher (0.3–0.6 MPa). Moreover, the H_2 pressure dependence of TOFs became less pronounced compared to those exhibited by small particles. In addition, the increase in H_2 pressure is accompanied by an increase in the reaction order with respect to CH partial pressure (Fig. S11), suggesting a decrease in the coverage of the CH-derived reactive species by increasing the chemical potential of H_2. It appears that small particles sense this H_2-pressure effect on coverage more strongly than the large particles.

Analyzing formation rates of different products separately in relation to the particle size and the H_2 pressure reveals marked differences (Fig. 6). Over small Ir particles, the formation rate of *n*-hexane exhibits a higher optimum H_2 pressure than the maxima of all other products (Fig. 6a). In contrast, the H_2 pressure dependence of *n*-pentane (and also methane) formation parallels that of *n*-hexane over large particles, both showing much higher optimal H_2 pressures than the other fragments (C_2–C_4) formed via internal multiple-scissions (Fig. 6b). The less pronounced dependence of the rate on H_2 pressure for *n*-hexane than for smaller alkanes leads in consequence to its enhanced selectivity at higher H_2 pressure on both small and large particles (Fig. 7a). The selectivity gap greater than 20% between small and large particles persists at all H_2 pressures studied (Fig. 7b), mainly due to the enhanced terminal hydrogenolysis on larger particles and the slightly divergent trends over small and large particles in response to the H_2 pressure increase. However, the selectivities to internal multiple cleavages consistently decrease with increasing H_2 pressure, hardly dependent on the particle size (Fig. 7c).

3.5. Temperature dependences of rates and selectivities over Ir particles of different sizes

Table 1 compiles the kinetic parameters for product formation routes (kinetic primary) at varying H_2 pressures over small and large Ir particles. The Arrhenius plots of TOFs for CH hydrogenolysis over typical small (D = 0.61) and large (D = 0.16) Ir particles are presented in Fig. S12. The $E_{a,app}$ decreased with particle size for each cleavage mode at the same conditions, but increased on the same particle size with increasing H_2 pressure. The $E_{a,app}$ for ring opening to *n*-hexane were 20–30 kJ mol^{-1} lower than for C_5 formation. Hydrogenolysis of internal C–C bonds had even higher activation energies than *n*-hexane and *n*-pentane formation. As a result, *n*-hexane selectivity decreased with increasing reaction temperature (Fig. S13, Supporting information). The slope of the *n*-hexane selectivity with the temperature showed that the selectivity shifts

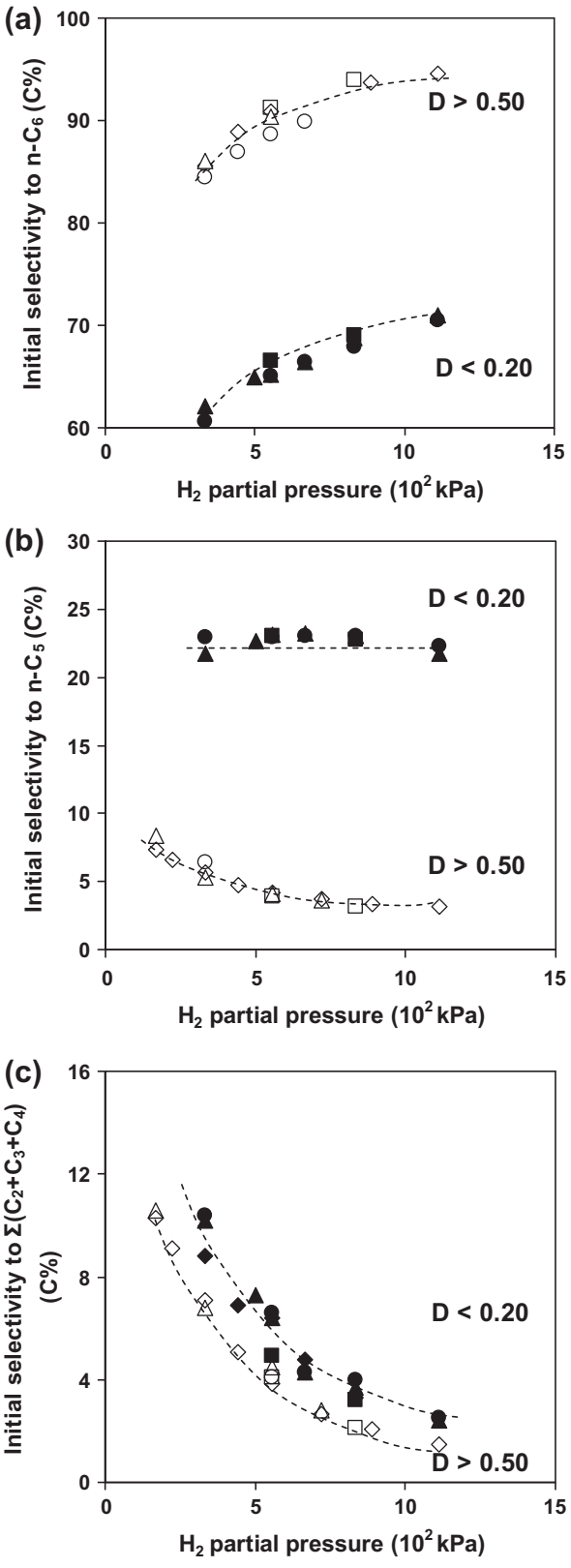

Fig. 7. Initial selectivities to (a) *n*-hexane, (b) *n*-pentane, and (c) lumped C_2–C_4 products as a function of H_2 pressure over small (D = 0.52–0.65) and large Ir particles (D = 0.014–0.16) at 523 K, 3.1 kPa CH.

were independent of the particle size. Also shown in Table 1, the typically larger activation energies for multiple hydrogenolysis on all particles and for all rates on small particles are compensated by the greater pre-exponential factors in the respective case. Compensation phenomena are common in the hydrogenolysis of alkanes [44]. Pre-exponential factors were similar on sufficiently large Ir particles (e.g., 10^7–10^8 s^{-1} for ring opening at 0.56 MPa H_2 on catalysts of D = 0.035–0.30).

4. Discussion

Hydrogenolysis of cyclohexane over these Ir catalysts yields *n*-hexane as the sole mechanistically primary product. Some *n*-hexane formed in this process undergoes multiple hydrogenolysis before vacating the surface. Consequently, a fraction of the smaller alkanes formed from these non-desorbed *n*-hexane molecules are discerned as apparent primary products due to their non-zero selectivities at zero contact time (Figs. 3 and S10).

4.1. Cleavage patterns of cyclohexane in primary and secondary pathways

Conceptually, as the concentration of available surface hydrogen (H^*) decreases, the ring-opened intermediate state has a higher chance of experiencing further C–C bond scissions before H^*-facilitated desorption. Thus, reaction variables that deplete the adsorbed hydrogen increase the selectivities to multiple C–C bond cleavage. The binding energy of H^* is higher on step edges than on terraces [45,46]. Consequently, the steady-state H^* coverage should be higher on small Ir particles with a relatively larger fraction of these defect sites compared to large ones [11,38]. This, in turn, suggests that the observed lower selectivity to hydrogenolysis of the intermediately formed *n*-hexane on small Ir particles (Fig. 4b) is related to higher H^* concentrations, in keeping with the proposal by Paál and coworkers [47]. Alternatively, the probability of finding neighboring sites to accommodate reactive states for multiple C–C bond scissions is expected to increase on terrace planes over large particles, resulting in lower RO selectivities.

Primary and secondary pathways showed different preferences to terminal and internal cleavage modes for multiple hydrogenolysis (Section 3.3.2). Based on the observed changes of product selectivities with contact time (Fig. 3), we infer that the active species derived from CH first undergoes a single C–C bond scission leading to adsorbed *n*-hexane. This intermediate has a certain probability of undergoing further cleavage of a terminal C–C bond, as well as a lower probability of hydrogenolysis at internal C_{II}–C_{II} (bi-secondary) bonds. This low selectivity to hydrogenolysis of internal C–C bonds is likely related to the interaction of the $C^{1,6}$-atoms in the proposed structure of the intermediate with the Ir surface (Scheme 2). Both interacting C-atoms might assume a sorbate configuration (probably through bonding at a threefold hollow site in a quite rigid sp^3 configuration) that renders access of inner carbon atoms ($C^{2,3,4,5}$) to neighboring metal atoms highly improbable. For achieving cleavage of the terminal C–C bond, only one of the $C^{1,6}$-atoms needs to be mobile via partial detachment from the surface (Scheme 2), while both Ir–C bonds need to become flexible for cleavage of an inner C–C bond. It was also observed that the apparent activation energies were significantly larger for products from internal C–C bond scissions, increasing progressively with increasing H_2 pressure (Table 1). This reflects the lower coverages of reactive species for multiple C–C bond scissions at internal positions and the greater suppression effects of H_2 pressure on their coverage.

On large Ir particles, the probability of terminal C–C bond cleavage in kinetic primary pathways is higher than that for hydrogenolysis of internal C–C bonds (Fig. 3b), whereas the difference between two modes is much smaller on small particles (Figs. 3a and S10a). This might point to the fact that on small particles the

Table 1
Kinetic parameters over Ir/Al_2O_3 catalysts with varying dispersions.

	H_2 pressure (10^2 kPa)	$E_{a,app}$ (kJ mol^{-1})[a]				Apparent pre-exponential factor, A_{app} (s^{-1})[b]			
		C_6	C_5	C_4	C_3	C_6	C_5	C_4	C_3
0.50%Ir(0.65)–1/Al_2O_3	3.3	121	147	175	187	8.2×10^{10}	2.6×10^{12}	8×10^{14}	3×10^{16}
	5.6	154	174	216	218	1.1×10^{14}	5.8×10^{14}	4×10^{18}	1×10^{19}
	11.1	179	199	–[c]	–[c]	1.1×10^{16}	4.3×10^{16}	–	–
0.50%Ir(0.52)–1/Al_2O_3	5.6	146	170	208	210	4.6×10^{12}	9.3×10^{13}	2×10^{17}	5×10^{17}
0.54%Ir(0.46)–2/Al_2O_3	3.3	116	145	155	158	2.9×10^{9}	1.6×10^{11}	2×10^{12}	5×10^{12}
	5.6	138	168	197	208	2.8×10^{11}	1.7×10^{13}	1×10^{16}	1×10^{17}
	11.1	158	180	–[c]	–[c]	8.3×10^{12}	7.0×10^{13}	–	–
0.54%Ir(0.30)–2/Al_2O_3	5.6	95	98	160	170	4.3×10^{7}	3.0×10^{7}	8×10^{12}	1×10^{14}
	11.1	102	118	176	210	1.8×10^{8}	2.5×10^{9}	1×10^{14}	2×10^{17}
0.50%Ir(0.16)–1/Al_2O_3	5.6	87	105	157	163	1.9×10^{7}	5.0×10^{8}	3×10^{12}	6×10^{12}
	8.3	95	117	167	200	1.1×10^{8}	7.1×10^{9}	5×10^{13}	1×10^{17}
0.50%Ir(0.035)–1/Al_2O_3	5.6	85	106	152	154	3.1×10^{7}	1.6×10^{9}	8×10^{12}	2×10^{13}
	8.3	94	116	169	185	2.2×10^{8}	1.4×10^{10}	2×10^{14}	1×10^{16}

[a] Reaction conditions were 3.1 kPa CH and 513–553 K; these reported values, with maximum error of ±5 kJ mol^{-1} for butanes and propane and ±3 kJ mol^{-1} for hexanes and pentanes, were derived by taking the slopes from semilogarithmic Arrhenius plots of formation rates of different products as a function of reciprocal temperature.
[b] The pre-exponential factors were derived from the r (TOF) = $A_{app} \times \exp(-E_{a,app}/RT)$. The errors depend on the accuracy of values for activation energies. Therefore, the relative standard deviation is ±30–60% for *n*-hexane and *n*-pentane and ±300–500% for *n*-butane and propane.
[c] These values are >200 kJ mol^{-1} but are likely overestimated due to the inaccuracy of the low extrapolated initial rates at lower temperatures.

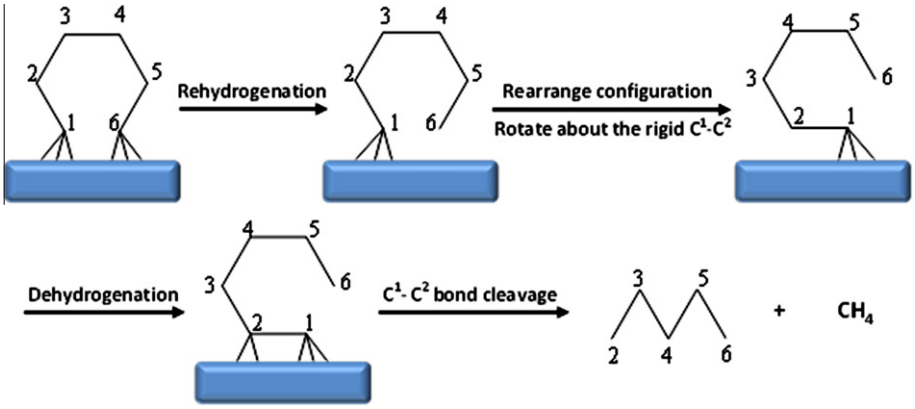

Scheme 2. Terminal C–C bond cleavage prevails in chemisorbed *n*-hexane intermediate formed from cyclohexane ring opening on flat surfaces (C^1–C^2 bond cleavage as an example). Carbon atoms at 2–5 positions in the starting molecule cannot access the surface effectively.

sp^3 configuration of the ring-opened intermediate is less favored (lower concentration of threefold hollow sites) than the more flexible bonding in twofold and in atop configurations [48]. As discussed above, the favorable adsorbed state after the first C–C bond scission enabling further hydrogenolysis is one in which a higher flexibility of the metal–carbon bond is assumed.

In stark contrast to kinetic primary pathways, less than 15 mol% of kinetic secondary C–C bond scission reactions yielded *n*-pentane/methane on small Ir particles, and only ca. 1–2 mol% on large particles (Figs. 3 and S10). As the secondary reactions largely bypassed the cleavage of a terminal C–C bond, the associated adsorbed states of *n*-hexane (primary products) directly reacting further and those formed upon its re-adsorption must be different from each other. This suggests that upon re-adsorption on the metal, the activation of the C–H bond in the *n*-hexane molecule on the surface becomes more important in affecting the C–C bond cleavage reactivities through the coverages of relevant intermediates.

4.2. Implications of H_2 pressure effects on product formation rates and apparent activation energies in cyclohexane hydrogenolysis

Although the surface concentration of H-adatoms (H^*) plays a crucial role in hydrogenolysis [49], a detailed mechanistic analysis under high H_2 pressures has been lacking. In the present work, the decrease in Ir dispersion, especially from high ($D > 0.50$) to low values ($D < 0.20$), shifts the optimal H_2 pressure to higher values and leads to less pronounced variations for primary ring opening (*n*-hexane) and for the subsequent terminal hydrogenolysis (*n*-pentane) on large (average size >5 nm) Ir particles. This is radically different from the steep decline after the rate maxima on small (1–2 nm) particles. It appears that small Ir particles respond to the H^* coverage variations more than large particles (Fig. S11), possibly reflecting that both CH-derived reactive species and H^* strongly compete for the low-coordination sites.

Alternatively, the concentrations of the H-deficient reactive intermediates and the concentration of vicinal H^* may dictate the H_2 pressure at which the maximum rate emerges. Conceptually, an increase in H^* coverage will decrease the population of such deeply dehydrogenated species. Therefore, we reason that the lower pressure dependence and the higher optimum H_2 pressures on large particles (Figs. 5b and 6b) point to a less H-deficient nature of the most abundant reactive intermediates (MARIs) than on small particles (for a more rigorous discussion, refer to Sections 4.4 and 4.5).

The functional relation between $E_{a,app}$ and reactant pressures was first derived by Temkin [50] and expressed as follows:

$$E_{a,app} = E_{a,int} + \Sigma n_i \Delta H_i \quad (1)$$

where n_i is the order in the reactant *i*. The enthalpy change for H_2 chemisorption is negative, and the reaction order in H_2 is also

negative after the optimum H_2 pressure. The activation (adsorption plus dehydrogenation) of cyclic hydrocarbons prior to C–C bond scission is endothermic (weaker C–M bonds than C–H bonds) when dissociated hydrogen atoms recombine and desorb as gas phase H_2 (i.e., no net effect from M–H bond strength), and the reaction order in CH is fractional and tends to unity with increasing H_2 pressures.

It follows from Eq. (1) that over much of the H_2 pressure range, $E_{a,app}$ would be greater than $E_{a,int}$. For catalysts of higher dispersions ($D \geqslant 0.46$), the reaction order in H_2 goes more negative at higher H_2 pressures, while the reaction order in CH stays always positive and increases with H_2 pressures, both factors weighing on the increase in apparent activation energies (Table 1). The slightly changed $E_{a,app}$ with increasing H_2 pressure for hydrogenolysis of CH over large Ir particles ($D < 0.20$) is qualitatively attributed to the lower sensitivity of the H_2 reaction order in the studied pressure range (Figs. 5 and 6 and S14). The markedly lower apparent activation barriers for primary C–C bond cleavage over the large Ir particles are attributed to the much smaller reaction orders in H_2 (−0.8 to 0.3) and in CH (0.2–0.5) compared to those (−2.5 to −0.8 and 0.4–0.7, respectively) exhibited by high-dispersion catalysts. These variations in reaction orders reflect a lower coverage of H-adatoms and a higher coverage of CH-derived intermediates on the surface of large particles than on small particles. The intrinsic barrier for CH hydrogenolysis on large particles was estimated to be 85 ± 10 kJ mol^{-1}, by applying Eq. (1) at conditions where reaction orders in H_2 and CH are both close to zero (e.g., at 523 K, 3.1 kPa CH, 0.5–0.6 MPa H_2). Despite that the precision of the Temkin equation may be questioned in fractional-reaction-order cases, the estimation was attempted also for results on small particles, which led to $E_{a,int}$ values typically larger than 100 kJ mol^{-1}. In comparison, kinetic modeling of rates at different temperatures (not shown) suggested that the intrinsic activation energy is about 100 ± 10 kJ mol^{-1} on small clusters, that is, 10–20% larger than the value for the large particles.

4.3. Mechanistic considerations based on a classical microscopic model for alkane hydrogenolysis

Before discussing the identity of active sites and catalytically relevant species that give rise to the observed structure sensitivities and H_2-pressure dependent kinetics for endocyclic C–C bond cleavage, we would like to first outline some mechanistic considerations. It is well accepted that the non-activated dissociative chemisorption of H_2 and the chemisorption of alkanes both remain quasi-equilibrated on the time scale of hydrogenolysis turnovers [4,51–57]. We propose that H* and reactive intermediates compete for the hydrogenolysis sites, a hypothesis seen valid in MCP and ethane hydrogenolysis over Pt and Ru catalysts, respectively [21,51].

A generalized catalytic sequence, involving quasi-equilibrated steps of H_2 and hydrocarbon activation, an irreversible C–C bond rupture rate-determining step (RDS), and kinetically insignificant re-hydrogenation and desorption steps, is shown in Scheme 3, and the derivation of the rate equation for this mechanistic sequence is shown in the Supporting information [58]. In a rigorous sense, the molecularity of the RDS remains elusive in hydrogenolysis reactions. Engstrom et al. suggested that the activated C–C bond breaks without involving other species or empty sites [12]. Zhuang and Frennet found that better fits in kinetic modeling of a rate expression were obtained when assuming a gas phase or weakly adsorbed H_2 molecule to be required in the RDS [21]. Shang and Kenney considered no less than ten rate equations and concluded that the involvement of an empty site in the RDS offered the best option for modeling their results on ethane hydrogenolysis over Ru/SiO_2 [51]. For the moment, let us be concerned with a more reasonable model for alkane hydrogenolysis as suggested by Bond [4] and considered by some others [21,51,53], with a few modifications of the original site balance equation (Supporting information). This model assumes a surface H* acting as the splitting agent in the rate-controlling C–C bond cleavage. Here, we consider that the H*-assisted RDS may be favored over the non-assisted C–C bond cleavage, which can be understood by kinetic coupling [59,60] of C–H bond formation in the transition state with the C–C bond cleavage that brings down the activation barrier.

The parity plots are shown in Fig. S15 for three mechanisms differing only in the RDS. Tables S2 and S3 present the four fitted parameters derived from non-linear regression analysis of measured CH hydrogenolysis rates at 523 K on Ir/Al_2O_3 catalysts containing small and large particles, respectively. We are aware that the mechanistic soundness of all assumptions is to be subjected to the scrutiny of further experimental studies as well as theoretical assessments. Note, however, that most of the other competing proposals lack precision in predicting the reaction order in CH compared to the "H*-assisted C–C bond cleavage" model (Fig. S16), and that the "vacancy-involved" RDS assumption results in much lower values of the H_2 adsorption constant (1.6×10^{-5} - kPa^{-1}) and the estimated coverage of H* (0.04–0.11) than the "H*-assisted" RDS assumption.

4.4. Structure sensitivity of cyclohexane hydrogenolysis: the sympathetic branch

The TOF of structure-sensitive reactions may decrease when the dispersion increases, which is defined as antipathetic structure sensitivity; if the TOF increases with increasing dispersion, the behavior is termed as sympathetic structure sensitivity [61]. There exist cases where the TOF passes through a maximum [61], whereas the contribution of Del Angel et al. showing that the TOF for MCP hydrogenolysis had a minimum with varying Rh dispersion [62] is the only case we have found in the literature where the TOF of a reaction passed through a minimum as a function of dispersion. In this and the next sections, we separately address the possible mechanistic and structural origins for the sympathetic and antipathetic branches of TOF variation with Ir dispersion in CH hydrogenolysis (Figs. 2b and S9) [63].

As expected from the closely resembled H_2 pressure dependences (Table S2, Supporting information) and the nearly equivalent H_2 pressure values at rate maxima on small particles (Fig. 5a), the differing TOFs should primarily stem from the scaling properties, that is, intrinsic rate constants of the RDS. Indeed, modeling results show that the thermodynamic properties (K_{cyc}, K_H, and x in Scheme 3) governing the equilibrium concentration and distribution of surface species do not vary to a substantial degree on high-dispersion catalysts ($D = 0.5–0.7$), as is also seen from the similar estimated coverages (Table S3). More remarkably, the number of C–H bonds cleaved before C–C bond scission is predicted to be nearly four ($x \approx 2$ (H_2 molecules)) on small particles of $D > 0.50$ (Table S3), which corresponds exactly to the widely proposed C_2-unit mode, or the so-called dicarbene structure over Ir [1,11,33,64].

Now that the observed structure sensitivity has been deprived of coverage effects, it becomes valid to base the interpretation of the sympathetic branch simply on the decrease in the RDS rate constant with increasing particle size. At the present stage, we consider that the population of low-coordination atoms is most consequential to catalysis, owing to their greater coordinative unsaturation. As first quantified by van Hardeveld and Hartog [65], the percentage of low-coordination atoms, among all types of surface atoms, decreases sharply in this narrow range (1–2 nm). Table 2 shows a quantitative estimation of the population of different types of surface atoms in closed-shell cuboctahedral Ir particles. For example, with a slight increase in particle size from

(i) H_2 chemisorption:

$$H_2\,(g) + 2^* \underset{}{\overset{K_H}{\rightleftharpoons}} 2H^* \qquad K_H = \frac{\theta_H^{\,2}}{P_H \theta_v^{\,2}}$$

(where * represents an unoccupied surface Ir atom; θ_V, θ_H are the vacancy coverage and H*-coverage, respectively)

(ii) Hydrocarbon activation (lumped with recombination of H^* into gas phase H_2):

$$c\text{-}C_6H_{12}\,(g) + n^* \underset{}{\overset{K_{cyc}}{\rightleftharpoons}} (c\text{-}C_6H_{12-2x})_n^{\#} + xH_2\,(g) \qquad K_{cyc} = \frac{\theta_{cyc} P_H^{\,x}}{P_{cyc} \theta_v^{\,n}}$$

(where θ_{cyc}, n and x are the coverage by the most abundant CH-derived surface intermediates, the number of free surface atoms and the depth of dehydrogenation; $^{\#}$ represents the adsorption site for cyclic hydrocarbon species, $c\text{-}C_6H_{12-2x}$, comprising n surface atoms and is thus different from *)

(iii) C–C bond cleavage (rate determining):

$$(c\text{-}C_6H_{12-2x})_n^{\#} + \text{`}\mathbf{S}\text{'} \xrightarrow{k_{rds}} (RO\text{-}C_6H_{12-2x})_n^{\#} \qquad R_{rds} = k_{rds}\,\theta_{cyc}\,['s']$$

(where $(RO\text{-}C_6H_{12-2x})_n^{\#}$ is a ring-opened state different from the cyclic state with the prefix 'c-'; x is the depth of dehydrogenation and '**S**' can be an empty site (*), an adsorbed hydrogen (H^*), molecular H_2, a combination of H_2 + *, or even non-existent for non-assisted C–C bond scission; 'S' was taken as H^* in the present study; any potential release of sites previously covered by 'S' is not shown on the product side)

(iv) Rehydrogenation and desorption (kinetically irrelevant steps, not necessarily quasi-equilibrated, can be reversible or irreversible):

$$(RO\text{-}C_6H_{12-2x})_n^{\#} + (2x{+}2)H^* \rightleftharpoons C_6H_{14}\,(g) + (2x + 2{+} n)^*$$

Scheme 3. Sequence of steps (not elementary for quasi-equilibrated steps) proposed for cyclohexane hydrogenolysis on Ir/Al_2O_3 catalysts.

1.6 to 2.2 nm, the percentage of corner atoms could reduce almost by a factor of 3. This magnitude is similar to the difference in rate constants, that is, a factor of 3–4, in this dispersion range (D = 0.52–0.65).

We anticipate that the activity would stop increasing and start to drop, with further increasing dispersion (D > 0.65), somewhere before D reaches unity, as a single surface-bound Ir atom is unlikely to accommodate the C–C bond and H-adatoms at the same time. To clarify this point, it would be highly relevant to study the catalytic performance of site-isolated mononuclear Ir complexes [66,67] and sub-nanoclusters [68,69] in the hydrogenolysis of cyclohexane. These well-defined structures have been investigated in alkene hydrogenation [66,67], but have not yet been explored in hydrogenolysis reactions which are more sensitive to surface structures and more demanding in reaction conditions.

4.5. Structure sensitivity of cyclohexane hydrogenolysis: the antipathetic branch

Large Ir particles employed in this work exhibit the following kinetic features. First, compared to the high-dispersion catalysts, the H_2 pressures for maximum rates are higher, and the suppression of activity by H_2 pressure after the optimum is less distinct (Fig. 5). Second, the reaction order in CH is lower than that measured over small particles (Fig. S11). Third, the temperature dependence of rates (i.e., $E_{a,app}$) is lower than in the case of high-dispersion catalysts (Fig. S12). As argued above, the first feature suggests a less-dehydrogenated nature of the catalytically relevant species for C–C bond cleavage on large particles. According to a Langmuir–Hinshelwood formalism, the second feature points to a higher equilibrium coverage of CH-derived reactive intermediates and/or a less severe competition with H^* adsorption sites. And the last feature can be understood from the Temkin relation as a result of smaller contributions from the exothermicity term for H_2 chemisorption and the endothermicity term for CH chemisorption. Consequently, the apparent energies of activation on large particles are close to the intrinsic activation barrier for C–C bond cleavage. Although it is tempting to ascribe the higher intrinsic rate constants on very large Ir particles to greater intrinsic pre-exponential factors (transition-state entropy changes), rather than to smaller activation barriers, the accuracy (±10 kJ mol^{-1}) of determining true activation barriers on small and large particles renders a conclusive statement difficult.

Compatible with the above qualitative analysis, dehydrogenation depths lower (x = 1.2–1.6) than those on small particles were predicted by kinetic modeling of TOFs measured on low-dispersion

Table 2
Estimated population of four types of surface atoms in a cuboctahedral model for four particle sizes (i.e., shell number: 3, 4, 5 and 6, respectively)[a].

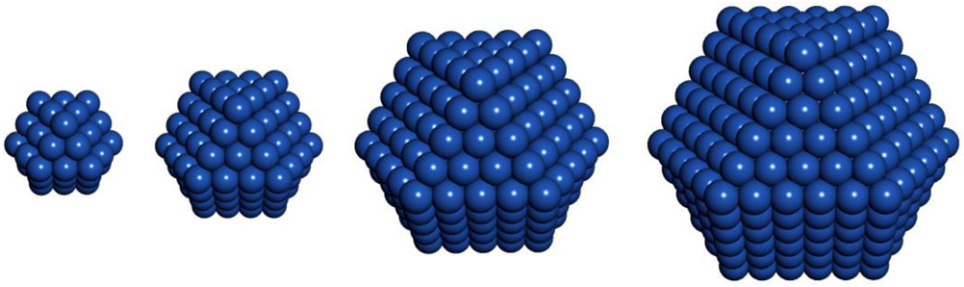

Type	CN	Fraction of surface atoms			
		Ir_{55} (1.3 nm, $D = 0.76$)[b]	Ir_{147} (1.6 nm, $D = 0.63$)[b]	Ir_{309} (1.9 nm, $D = 0.52$)[b]	Ir_{561} (2.2 nm, $D = 0.45$)[b]
Corner	5	0.286	0.130	0.074	0.048
Edge	7	0.571	0.521	0.444	0.381
(100)	8	0.143	0.261	0.333	0.381
(111)	9	0	0.087	0.148	0.190

[a] Numerical formulae: N_s (number of surface atoms) = $10m^2 - 20m + 12$; N_{corner} (number of corner atoms) = 12; N_{edge} (number of edge atoms) = $24(m-2)$; $N_{(100)}$ (number of (100) terrace atoms) = $6(m-2)^2$; $N_{(111)}$ (number of (111) terrace atoms) = $4(m-3)(m-2)$.
[b] D (dispersion) = N_s/N_t, d (Ir particle size) ≈ $0.99/D_{Ir}$ [42].

catalysts when the same mechanistic sequence was applied (Table S4, Supporting information). The dehydrogenation depth could be even less pronounced (smaller x), if the adsorption strength of H* on these large particles had been underestimated by kinetic modeling. Any attempts to constrain the dehydrogenation depth at $x = 2$ and model the other three parameters only lead to unreasonable estimates of H* adsorption equilibrium constant and H* coverage (Table S5, Supporting information). It is interesting to note that Engstrom et al. [12] explained the differences in the apparent reaction kinetics and pre-exponential factors of ethane hydrogenolysis on Ir(111) and Ir(110)-(1 × 2) surfaces also by different reaction intermediates, namely, C_2H_4(ads) on the former and C_2H_2(ads) on the latter. That is, an extensively dehydrogenated species was the MARI on the Ir(110)-(1 × 2) surface containing a large faction (25%) of low-coordination atoms, while a less unsaturated species was the MARI on terrace sites. The underlying driving forces for various surface structures to effect different H-deficiencies of MARIs may root in the different degrees of coordinative unsaturation of surface atoms.

The antipathetic structure sensitivity is ascribed to a less unsaturated and more reactive nature of the carbonaceous MARI and possibly also an adsorption mode that requires a larger ensemble size than the dicarbene-like adsorption complex prevalent on small particles. It is possible that an adsorption state parallel to the surface exists on large Ir particles predominantly terminated with terrace planes. Although the (111) and (100) planes also exist on small particles, the large ensemble size requirement for the adsorption parallel to the surface would make this mode nearly inoperative on high-dispersion catalysts.

To the best of our knowledge, there has been no literature on the structure sensitivity of CH hydrogenolysis over supported Ir catalysts or model Ir surfaces. Surface science studies by Somorjai and coworkers were one of the few investigations into structure sensitivity of CH hydrogenolysis on metal surfaces [16–18]. Over different Pt model surfaces, these authors showed that Pt(111) terraces without steps and kinks are the most active for C–C bond breaking of CH in 15 Torr CH and 100 Torr H_2 [16], opposite to the trend observed by the same group at very low CH (5×10^{-6} Pa) and H_2 (10^{-4} Pa) pressures where kinks in the steps appeared the most active [17,18]. These surface science studies seem to suggest both surface structures to be active for the C–C bond hydrogenolysis, and that this apparent contradiction can be resolved by the different reaction conditions applied. While being intrinsically active for C–C bond cleavage, low-coordination atoms might have been irreversibly titrated by carbon deposits when CH coverage was high, as in the former case [16], rendering them inactive in catalytic turnovers. In the present work, these coordinatively unsaturated atoms are still active on small Ir particles, because Ir possesses much higher hydrogenolysis activity than Pt, and so, is more resistant to carbon deposition.

4.6. H-deficiency of reactive intermediates as the selectivity mediator for single-scission and terminal/internal multiple-scissions

We interpret here the effects of H_2 pressure on the ring opening selectivity (Fig. 7) on the basis of the unsaturation degree of surface intermediates. Within the framework of the kinetic model (Scheme 3), we introduce different H-deficiencies (the value of x) of MARIs for single and multiple C–C bond scissions (denoted as S_{RO} and S_{multi}, respectively) and also for internal and terminal modes of multiple-scissions (denoted as S_{tm} and S_{im}, respectively). According to step (iii) in Scheme 3, the formation rates of single-scission (RO) product and multiple-scission products along kinetic primary pathways are given by the rates of the C–C bond cleavage:

$$r_{RO} = k_{RO}\theta_{S_{RO}}\theta_H \tag{2}$$

$$r_{multi} = k_{multi}\theta_{S_{multi}}\theta_H \tag{3}$$

The quasi-equilibrium assumption for cyclohexane activation (step ii, Scheme 3) implies that the MARIs for single and multiple C–C bond cleavage in kinetic primary pathways also exist in equilibrium:

$$S_{RO} \rightleftharpoons S_{multi} + (x_{multi}\text{-}x_{RO})\ H_2 \tag{4}$$

where x_{RO} and x_{multi} refer to the dehydrogenation depths of the MARIs for single and multiple C–C bond cleavage, respectively, and, thus, gives:

$$\theta_{S_{RO}} = K_{int}^{-1}\theta_{S_{multi}}P_H^{(x_{multi}-x_{RO})} \tag{5}$$

where K_{int} is defined as the equilibrium constant for Eq. (4). Thus, a functional relation (Eq. (6)) can be established between H_2 pressure

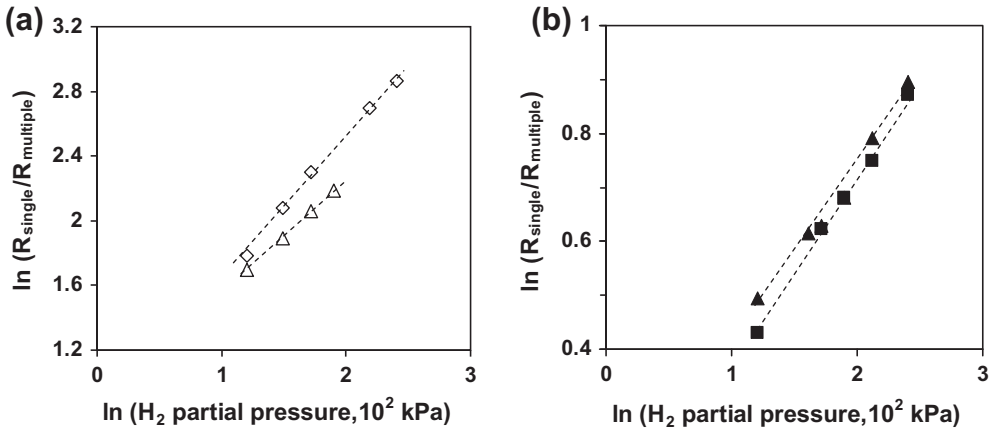

Fig. 8. Different H-deficiencies of MARIs for single-scission (RO) and multiple-scissions indicated by the dependences of rate ratios on H_2 pressure over (a) small ($D > 0.50$, ◇△) and (b) large ($D < 0.20$, ■▲) Ir particles. Reaction conditions: 523 K, 3.1 kPa CH.

and the rate ratio of single and multiple hydrogenolysis (detailed derivation in Supporting information).

$$\ln\left(\frac{r_{RO}}{r_{multi}}\right) = \ln\left(\frac{k_{RO}}{k_{multi}K_{int}}\right) + (x_{multi} - x_{RO})\ln P_H \quad (6)$$

Therefore, the slope of the $\ln(r_{RO}/r_{multi}) - \ln(P_H)$ plot points to the difference in the H-deficiency between surface intermediates involved in single and multiple C–C bond scissions, respectively. The double-logarithmic function is plotted in Fig. 8 for both small and large Ir particles. A comparison of the slopes in Fig. 8a and b indicates that H-deficiency (x) is less different between S_{RO} and S_{multi} on large than on small particles, thus bringing the reactivities of single and multiple C–C bond scissions closer together (Fig. 6b). As is shown in a quantitative way (Table 3), the active intermediate for ring opening possibly has to further lose more than one hydrogen atom, on average, to allow multiple hydrogenolysis on small Ir particles, in accordance with a previous report on the hydrogenolysis of lower alkanes over Ru/Al_2O_3 catalysts [70].

In contrast, less than one hydrogen needs to be further abstracted for multiple-scission to occur on large particles before desorption of the ring-opened intermediate (Table 3). Moreover, the average H-deficiency of active intermediates for internal multiple-scission is greater than single-scission (RO) and terminal multiple-scission on both small and large particles, accounting for their lower values of H_2 pressure at maximum rates in primary reactions (propane and butane in Fig. 6) and the constantly decreasing selectivity to internal multiple-scission with increasing H_2 pressure (Fig. 7c). The rates of those pathways that have greater dehydrogenation depths before C–C bond rupture exhibit more marked suppression by increasing H_2 pressure (Fig. 6). The greater dehydrogenation depths at internal C–C bonds can be attributed to the slightly weaker secondary C–H bonds [71]. Finally, a deeper unsaturation degree of S_{im} than S_{RO} and S_{tm} would necessitate a higher contribution of the endothermicity term in the Temkin relation (Eq. (1)), leading to higher apparent activation energies for internal hydrogenolysis (Table 1).

Table 3
Different extents of H-deficiency of reactive intermediates for single-scission, terminal and internal multiple-scissions at 523 K on typical small and large Ir particles.

$x_m - x_{RO}$ (H-deficiency difference)[a]	$D = 0.65$	$D = 0.16$
Terminal multiple-scission	0.5–0.6	0.1–0.2
Internal multiple-scission	0.9–1.0	0.4–0.6

[a] The difference in dehydrogenation depth (x) of reactive intermediates between single-scission and multiple-scission (including terminal and internal).

5. Conclusions

The present study investigates Ir catalysts of varying dispersions, without the presence of a solid acid, that catalyze exclusively the direct C–C bond cleavages of cyclohexane.

A dual-branch sensitivity of the TOFs to the Ir dispersion ($D = 0.01–0.65$) was observed for the C–C bond cleavage. The sympathetic structure sensitivity originates from the declining population of low-coordination atoms leading to lower rates. On the basis of the measured reaction barriers, the Temkin relation and modeling results, we conclude that reactive intermediates of smaller H-deficiency are involved in the rate-limiting C–C bond cleavage on low Ir dispersion catalysts. It is also speculated that a new adsorption mode of cyclohexane that requires a sizable ensemble is more favorably formed on terrace planes.

The pathways for multiple hydrogenolysis in kinetically primary and secondary reactions differ greatly. The relative importance of the pathways depends mainly on the Ir particle size and H_2 pressure and to a lesser degree on the reaction temperature in the studied range. The detrimental effects of lower H_2 pressures, larger particle size, and higher temperatures on the selectivity to *n*-hexane are mainly attributed to the nature of reactive intermediate for single and multiple C–C bond cleavage, as well as the availability of adsorbed vicinal hydrogen species. The generally high values of apparent energies of activation for hydrogenolysis (that further increase with increasing H_2 pressure) are a consequence of the endothermic activation of cyclic reactants. Moreover, the even higher activation energies for internal C–C bond cleavages are attributable to an energetically more demanding nature as well as a low coverage of the reactive intermediates involved in the rate-determining step.

Acknowledgments

Hui Shi thanks the Elitenetzwerk Bayern NanoCat for a Ph.D. grant and financial support. The authors are indebted to Dipl.-Ing. Xaver Hecht for the help with construction of the reactor setup and for conducting N_2 physisorption and H_2 chemisorption measurements. Skillful assistances from Dr. Marianne Hanzlik (Technical university of Munich, Germany) and Dr. Andrew DelaRiva (University of New Mexico, USA) are gratefully acknowledged during the TEM measurements. We also thank

Dr. George D. Meitzner (Edge Analytical, Inc.) for his critical reading of the manuscript.

Appendix A. Supplementary material

Supplementary data associated with this article can be found, in the online version, at http://dx.doi.org/10.1016/j.jcat.2012.08.005.

References

[1] G.B. McVicker, M. Daage, M.S. Touvelle, C.W. Hudson, D.P. Klein, W.C. Baird Jr., B.R. Cook, J.G. Chen, S. Hantzer, D.E.W. Vaughan, E.S. Ellis, O.C. Feeley, J. Catal. 210 (2002) 137.
[2] A. Corma, V. González-Alfaro, A.V. Orchillés, J. Catal. 200 (2001) 34.
[3] H. Du, C. Fairbridge, H. Yang, Z. Ring, Appl. Catal. A 294 (2005) 1.
[4] G.C. Bond, Metal-Catalysed Reactions of Hydrocarbons, Springer, Berlin, 2005.
[5] J.H. Sinfelt, J.L. Carter, D.J.C. Yates, J. Catal. 24 (1972) 283.
[6] H. Song, R.M. Rioux, J.D. Hoefelmeyer, R. Komor, K. Niesz, M. Grass, P. Yang, G.A. Somorjai, J. Am. Chem. Soc. 128 (2006) 3027.
[7] R.M. Rioux, H. Song, J.D. Hoefelmeyer, P. Yang, G.A. Somorjai, J. Phys. Chem. B 109 (2005) 2192.
[8] J.R. Anderson, B.G. Baker, Proc. Roy. Soc. A 271 (1963) 402.
[9] D.J.C. Yates, J.H. Sinfelt, J. Catal. 8 (1967) 348.
[10] D.E. Resasco, G.L. Haller, J. Catal. 82 (1983) 279.
[11] K. Foger, J.R. Anderson, J. Catal. 59 (1979) 325.
[12] J.R. Engstrom, D.W. Goodman, W.H. Weinberg, J. Am. Chem. Soc. 110 (1988) 8305.
[13] J.R. Engstrom, D.W. Goodman, W.H. Weinberg, J. Am. Chem. Soc. 108 (1986) 4653.
[14] D.W. Goodman, Catal. Today 12 (1992) 189.
[15] J. Barbier, P. Marecot, Nouv. J. Chim. 5 (1981) 393.
[16] R.K. Herz, W.D. Gillespie, E.E. Peterson, G.A. Somorjai, J. Catal. 67 (1981) 386.
[17] G.A. Somorjai, D.W. Blakely, Nature 258 (1975) 580.
[18] D.W. Blakely, G.A. Somorjai, J. Catal. 42 (1976) 181.
[19] F.G. Gault, Adv. Catal. 30 (1981) 1.
[20] M. Chow, G.B. McVicker, J. Catal. 112 (1988) 290.
[21] Y. Zhuang, A. Frennet, Appl. Catal. A 134 (1996) 37.
[22] D. Teschner, K. Matusek, Z. Paál, J. Catal. 192 (2000) 335.
[23] M. Vaarkamp, P. Dijkstra, J. van Grondelle, J.T. Miller, F.S. Modica, D.C. Koningsberger, R.A. van Santen, J. Catal. 151 (1995) 330.
[24] W.E. Alvarez, D.E. Resasco, J. Catal. 164 (1996) 467.
[25] M. Chow, S.H. Park, W.M.H. Sachtler, Appl. Catal. 19 (1985) 349.
[26] P. Samoila, M. Boutzeloit, C. Especel, F. Epron, P. Marécot, J. Catal. 276 (2010) 237.
[27] D. Kubička, N. Kumar, P. Mäki-Arvela, M. Tiitta, V. Niemi, H. Karhu, T. Salmi, D.Y. Murzin, J. Catal. 227 (2004) 313.
[28] D. Kubička, N. Kumar, P. Mäki-Arvela, M. Tiitta, V. Niemi, T. Salmi, D.Y. Murzin, J. Catal. 222 (2004) 65.
[29] S. Lecarpentier, J. van Gestel, K. Thomas, J.-P. Gilson, M. Houalla, J. Catal. 254 (2008) 49.
[30] M. Santikunaporn, J.E. Herrera, S. Jongpatiwut, D.E. Resasco, W.E. Alvarez, E.L. Sughrue, J. Catal. 228 (2004) 100.
[31] S. Rabl, A. Haas, D. Santi, C. Flego, M. Ferrari, V. Calemma, J. Weitkamp, Appl. Catal. A 400 (2011) 131.
[32] S. Nassreddine, L. Massin, M. Aouine, C. Geantet, L. Piccolo, J. Catal. 278 (2011) 253.
[33] P.T. Do, W.E. Alvarez, D.E. Resasco, J. Catal. 238 (2006) 477.
[34] J.-W. Park, K. Thomas, J. van Gestel, J.-P. Gilson, C. Collet, J.-P. Dath, M. Houalla, Appl. Catal. A. 388 (2010) 37.
[35] S. Nassreddine, G. Bergeret, B. Jouguet, C. Geantet, L. Piccolo, Phys. Chem. Chem. Phys. 12 (2010) 7812.
[36] G.B. McVicker, R.T.K. Baker, R.L. Garten, E.L. Kugler, J. Catal. 65 (1980) 207.
[37] S. Krishnamurthy, G.R. Landolt, H.J. Schoennagel, J. Catal. 78 (1982) 319.
[38] B.J. Kip, F.B.M. Duivenvoorden, D.C. Koningsberger, R. Prins, J. Catal. 105 (1987) 26.
[39] S. Brunauer, P.H. Emmett, E. Teller, J. Am. Chem. Soc. 60 (1938) 309.
[40] S. Balcon, S. Mary, C. Kappenstein, E. Gengembre, Appl. Catal. A 196 (2000) 179.
[41] H. Lieske, G. Lietz, H. Spindler, J. Volter, J. Catal. 81 (1983) 8.
[42] M. Choi, Z. Wu, E. Iglesia, J. Am. Chem. Soc. 132 (2010) 9129.
[43] M. Boudart, G. Djega-Mariadassou, The Kinetics of Heterogeneous Catalytic Reactions, Princeton University Press, Princeton, NJ, 1984.
[44] G.C. Bond, M.A. Keane, H. Kral, J.A. Lercher, Chem. Rev. Sci. Eng. 42 (2000) 323.
[45] B.E. Nieuwenhuys, D.I. Hagen, G.A. Somorjai, Surf. Sci. 59 (1976) 155.
[46] M.K. Oudenhuijzen, J.A. van Bokhoven, J.T. Miller, D.E. Ramaker, D.C. Koningsberger, J. Am. Chem. Soc. 127 (2005) 1530.
[47] A. Majesté, S. Balcon, M. Guérin, C. Kappenstein, Z. Paál, J. Catal. 187 (1999) 486.
[48] Alternatively, this difference can be attributed to the higher concentration of more reactive under-coordinated surface Ir atoms (corners, edges) on smaller Ir particles which discriminate less between the difficulties to cleave the first C–H bond than the sites with higher coordination on the surface of larger particles.
[49] V. Ponec, P.G. Menon, Catal. Rev. Sci. Eng. 25 (1983) 229.
[50] M. Temkin, Acta Phsiocochim. URSS 3 (1935) 312.
[51] S.B. Shang, C.N. Kenney, J. Catal. 134 (1992) 134.
[52] J.H. Sinfelt, D.J.C. Yates, J. Catal. 8 (1967) 82.
[53] J.H. Sinfelt, Catal. Rev. Sci. Eng. 9 (1974) 147.
[54] G.C. Bond, R.H. Cunningham, J. Catal. 166 (1997) 172.
[55] S.A. Goddard, M.D. Amiridis, J.E. Rekoske, N. Cardona-Martinez, J.A. Dumesic, J. Catal. 117 (1989) 155.
[56] A. Cimino, M. Boudart, H. Taylor, J. Phys. Chem. 58 (1954) 796.
[57] D.J.C. Yates, J.H. Sinfelt, W.F. Taylor, J. Am. Chem. Soc. 86 (1964) 2996.
[58] It is implied in the kinetic treatment that the most abundant surface intermediates are directly involved, not as spectators, in the primary reaction pathways. Competitive adsorption of two reactants is reflected in the site balance.
[59] M. Boudart, J. Phys. Chem. 87 (1983) 2786.
[60] M. Boudart, G. Djega-Mariadassou, Catal. Lett. 29 (1994) 7.
[61] M. Che, C.O. Bennett, Adv. Catal. 36 (1989) 55.
[62] G.A. Del Angel, B. Coq, G. Ferrat, F. Figueras, S. Fuentes, Surf. Sci. 156 (1985) 943.
[63] The ensemble size requirement for the C_2-unit mode must have been met on clusters of $D = 0.5–0.7$. Otherwise, it would have been rendered impossible to have the TOF increase as dispersion increases. It is also implied that there would be a maximum to be observed as the Ir dispersion tends further towards unity.
[64] F. Garin, G. Maire, Acc. Chem. Res. 22 (1989) 100.
[65] R. van Hardeveld, F. Hartog, Surf. Sci. 15 (1969) 189.
[66] J. Lu, P. Serna, C. Aydin, N.D. Browning, B.C. Gates, J. Am. Chem. Soc. 133 (2011) 16186.
[67] A. Uzun, V. Ortalan, N.D. Browning, B.C. Gates, J. Catal. 269 (2010) 318.
[68] A. Uzun, D.A. Dixon, B.C. Gates, ChemCatChem 3 (2011) 95.
[69] A.M. Argo, J.F. Odzak, B.C. Gates, J. Am. Chem. Soc. 125 (2003) 7107.
[70] G.C. Bond, J.C. Slaa, J. Mol. Catal. A 98 (1995) 81.
[71] D.F. McMillen, D.M. Golden, Ann. Rev. Phys. Chem. 33 (1982) 493.